Applied Catalysis B: Environmental 184 (2016) 12–19

Contents lists available at ScienceDirect

Applied Catalysis B: Environmental

journal homepage: www.elsevier.com/locate/apcatb

Carbon-supported Pt-free catalysts with high specificity and activity toward the oxygen reduction reaction in acidic medium

Luis Miguel Rivera Gavidia[a], Gonzalo García[a,*], Dalila Anaya[a], Amaia Querejeta[b], Francisco Alcaide[b], Elena Pastor[a,*]

[a] Instituto de Materiales y Nanotecnología, Departamento de Química, Universidad de La Laguna, Avda. Astrofísico Francisco Sánchez s/n, 38071 La Laguna, Santa Cruz de Tenerife, Spain
[b] División de Energía, IK4-CIDETEC, P° Miramón, 196, 20009 San Sebastián, Spain

ARTICLE INFO

Article history:
Received 21 July 2015
Received in revised form 6 November 2015
Accepted 16 November 2015
Available online 28 November 2015

Keywords:
ORR
DMFC
Catalysis
Pt-free catalysts
Specificity

ABSTRACT

Specific carbon-supported Pt-free catalysts (Pd, PdFe, PdIr and PdFeIr) toward the oxygen reduction reaction (ORR) were developed. With this end, materials with high and low activity toward the ORR and the methanol oxidation reaction (MOR) were synthesized by the borohydride method (BM). Physicochemical characterization was carried out by several x-ray techniques, such as x-ray photoelectron spectroscopy (XPS), x-ray diffraction (XRD) and x-ray dispersive energy (EDX). The ORR was studied at these materials in absence and presence of methanol in acidic medium in a half-cell configuration by the rotating disk electrode (RDE) technique. Additionally, the performance of the catalysts was evaluated as cathode material in a direct methanol fuel cell (DMFC) station. Main results indicate enhanced catalysis toward the ORR and improved tolerance toward the methanol by Fe and Ir insertion into the material, respectively. Membrane electrode assembly (MEA) with a cathode containing PdFeIr/C catalyst yields elevated performance in DMFC, while the electrode cost is dramatically reduced.

1. Introduction

Direct methanol fuel cells (DMFCs) are devices that convert efficiently chemical energy into electrical energy through electrochemical reactions while the fuel is supplied [1]. In this sense, DMFC emerges as an alternative technology to efficiently generate clean energy for portable applications [2,3]. Main advantages include high-energy density (6.1 kWh kg^{-1}), high solubility in liquid electrolytes, easy handling, transport, storage and availability at low cost [4,5]. Furthermore, the liquid-feed system does not require any reforming process that is time and cost consuming, as well as, the humidification and the heat management modules are much simplified compared with the proton exchange membrane fuel cell (PEMFC) due to methanol aqueous solution can provide the necessary heat control and humidification [4,6].

Despite the important advantages of DMFCs as power sources, a real DMFC has several drawbacks, being the crossover of methanol through the electrolyte from the anode to the cathode one of the major practical problems limiting the overall performance [7,8]. The simultaneous methanol oxidation and oxygen reduction reactions at the cathode produce the well known mixed potential that reduces the cell voltage, rises the required oxygen stoichiometry ratio, produces additional water and contaminates the Pt-based catalyst by reaction intermediates of the methanol oxidation reaction (e.g., CO_{ad}) [7–9].

A common strategy to overcome the problems associated to the cathode described above is the use of alternative materials to Pt. This ideal material should decrease the catalysts cost and increase the methanol tolerance without loss of catalytic activity toward the oxygen reduction reaction (ORR) [9]. In this context, Pd and Pd-based alloys appear as an interesting candidate to replace Pt due to its lower price and higher abundance [10–16]. In this sense, numerous studies demonstrated the high and low activity of Pd toward the ORR and methanol oxidation reaction (MOR), respectively [11–21]. However, the catalytic activity toward the ORR in acidic solution is much lower for Pd than Pt [22,23]. Thus, specific catalysts with enhanced activity toward the ORR in conjunction with a high methanol tolerance become necessary.

It is well known that many surface chemical reactions, such as the MOR and the ORR, are structure sensitive [15,23]. So, the surface reaction may be tuned by different factors such as changes in the interatomic distance of the active element (e.g., Pt or Pd), the

* Corresponding authors. Fax: +34 922 318002.
E-mail addresses: ggarcia@ull.edu.es, gonau111@gmail.com (G. García), epastor@ull.edu.es (E. Pastor).

http://dx.doi.org/10.1016/j.apcatb.2015.11.021
0926-3373/

composition of the alloy, the surface area, and the electronic configuration of the material [22–26]. In this way, the rate of a specific reaction could be controlled by the strength of the binding energy of the reactant molecule with the catalytic surface.

Some examples comprise Pd-based alloys (Fe, Ir, Ni, Ag and Co), in which higher activity and stability than pure Pd electrode during the ORR in presence of alcohol in the electrolytic medium were observed [16,19,24–32]. Likewise, well-dispersed PdIr nanoparticles on carbon support developed acceptable performances during the ORR [21]. Also, the effect of temperature treatment at carbon-supported catalysts was investigated. PdCo [13,33] and PdFe alloys [32,34] supported on carbon developed similar ORR performances than carbon supported Pt catalyst after a thermal treatment at 350 °C. On the other hand, fundamental studies using Pd(111) single crystal modified with a Pt monolayer obtained by galvanic replacement of Cu, showed an enhancement for the ORR in comparison with Pt(111) [35]. In the last work the mass specific activity (Pt + Pd) was twice higher than that of Pt/C. Additionally, Pd and Pd-based catalysts have been used as cathode in real fuel cell systems. In these experiments, the DMFC response was observed to depend on several factors, such as Pd loading and its interaction with the carbon support [23].

In the present work, carbon-supported Pd and Pd-based alloys (PdFe, PdIr, PdFeIr) were synthesized by the borohydride method (BM). Physicochemical characterization was carried out by several X-ray techniques, such as X-ray photoelectron spectroscopy (XPS), X-ray diffraction (XRD) and X-ray dispersive energy (EDX). Their electro-catalytic activity toward the ORR in absence and presence of methanol was carried out in a half-cell configuration; meanwhile their performance as cathode material was evaluated in a DMFC station.

2. Experimental

2.1. Catalyst synthesis

Carbon-supported Pd/C, PdFe(3:1)/C, PdIr(3:1)/C and PdFeIr(2:1:1)/C were prepared by the BM [36]. Appropriate amounts of metal precursors ($IrCl_3$, $FeCl_3.4H_2O$ and $PdCl_2$, Sigma–Aldrich) were employed to obtain nominal metal loading of 20 wt.% on carbon Vulcan XC-72-R. The materials were labeled as Pd/C, PdFe/C, PdIr/C and PdFeIr/C.

Catalysts were synthesized by the impregnation method, in which a suspension of carbon Vulcan XC-72R in milli-Q water (Millipore system) is prepared under ultrasonic bath and posteriorly stirred during ca. 24 h. Then, a water solution containing the metal precursors was slowly added to the carbon solution, and later the pH was adjusted to 5 with a saturated sodium hydroxide solution. Subsequently, metal ions were reduced with a 26.5 mM sodium borohydride (99%, Sigma–Aldrich) solution, which was slowly added under sonication and controlled temperature of 20 °C. Finally, catalysts were filtered and washed copiously with ultra pure water and dried at ca. 80 °C overnight.

2.2. Physicochemical characterization

X-ray diffractograms (XRD) of the electrocatalysts were obtained with a PANalytical X'Pert Pro X-ray diffractometer operating with Cu Kα radiation (λ = 0.15406 nm) generated at 40 kV and 20 mA. Scans were done at 0.04° s^{-1} for 2θ values between 20° and 100°. In order to estimate the particle size from XRD, the Scherrer equation was used [37]. With the purpose to improve the fitting of the peak, diffractograms for specific 2θ values ranges were recorded at 0.028 min^{-1}. The lattice parameters were obtained by refining the unit cell dimensions by the least squares method [38].

The atomic composition of the electrocatalysts was determined by energy dispersive X-ray analysis (EDX) coupled to the scanning electron microscopy Jeol JSM 6300 with a silicon doped with lithium 6699 ATW detector applying 20 keV.

X-ray photoelectron spectroscopy (XPS) analysis was performed with a Thermo-Scientific apparatus operating with Al Kα line radiation (1486.6 eV), containing a twin crystal monochromator and yielding a focused X-ray spot with a diameter of 400 μ at 3 mA × 12 kV. The alpha hemispherical analyzer was operated in the constant energy mode with survey scan pass energies of 200 eV to measure the whole energy band, and 50 eV in a narrow scan to selectively measure the particular element range. Charge compensation was achieved with the flood gun system that provides low energy electrons and argon ions from a single source. The samples were placed into a pre-chamber during 4–5 h. The analysis chamber pressure during the measurement was maintained below 5×10^{-8} mbars. The binding energies (BE) were calibrated relative to the C 1s peak at 284.6 eV to take into account charge effects. The areas of the peaks were calculated by fitting the experimental spectra using gaussian/lorentzian combined shapes, after the elimination of background noise upon use of Shirley-type curves. The surface atomic contents for each component were calculated from such fittings, employing the corresponding atomic sensitivity factors.

2.3. Electrochemical measurements

All measurements were carried out in a three-electrode cell at room temperature (25 °C) controlled by an Autolab PGSTAT302N potentiostat–galvanostat. A carbon row was used as a counter electrode, while the reference electrode was a reversible hydrogen electrode (RHE) in the supporting electrolyte (0.5 M H_2SO_4, Merck p.a.). All potentials are referred to this electrode. A rotating electrode (RDE) with a glassy carbon disk (geometrical area = 0.071 cm^2) was used. An aliquot of catalyst ink (20 μL) was dried onto the glassy carbon disk under Ar atmosphere to be used as working electrode. The suspension was prepared by stirring 2 mg of catalyst with 15 μL of Nafion® (5%, Sigma–Aldrich) and 500 μL of water (Milli-Q, Millipore). Ar (Air Liquide 99.999%) was used to deoxygenate all solutions and O_2 (Air Liquide 99.995%) to perform the measurements related to the ORR.

Previous to the measurements an activation step of the working electrode was performed. The last consists of potentiodynamic cycles between 0.10 and 0.70 V at 0.20 V s^{-1} in the supporting electrolyte until a reproducible voltammogram was achieved. Then, a blank cyclic voltammogram (BCV) was recorded at 0.02 V s^{-1}. For the ORR experiments, O_2 was bubbled 20 min before each experiment and an oxygen atmosphere was maintained during all measurements. Steady state polarization curves were recorded between 1.00 and 0.20 V at rotating speeds of 400, 600, 900, 1600 and 2500 rpm to evaluate the ORR kinetic parameters. In this study, the working electrode was introduced into the electrolyte at a controlled potential of 1 V and subsequently a linear sweep scan (LSS) was initiated in the negative going direction at scan rate of 0.002 V s^{-1}. The voltammetric profiles of the catalyst and the ORR experiments were studied in absence and presence of methanol in solution. With this end, 0.5, 1, 2 and 3 M methanol solution in 0.5 M sulphuric acid medium were employed.

2.4. Membrane electrode assembly preparation and electrochemical characterization

20 wt.% PdX/C (X = Pt and FeIr) and commercial 20 wt.% PtRu (Premetek Co, USA) on Vulcan® XC72R (Cabot Corp.) catalysts were used for the cathode and the anode, respectively.

Porous diffusion electrodes used to prepare MEAs consist of a diffusion layer and a catalyst layer. The gas diffusion layers were carbon papers covered on top with a carbon-based smooth layer (thickness 275 μm, Freudenberg FCCT SE & Co. KG). Electrodes prepared with carbon supported PtRu/C catalyst 71.5 wt.% metal loading and Pt:Ru atomic ratio 50:50 (Alfa Aesar) were used as anode. 20 wt.% metal loading of commercial Pd/C and $Pd_{25}Pt_{75}$/C (Premetek Co, USA), as well as, synthesized PdFeIr/C catalyst were used as cathode. For each catalyst layer, an ink was prepared by suspending the catalyst in water and 5 wt.% Nafion® ionomer dispersion (Aldrich) in a mixture of isopropanol (Acros Organics, pur.) and ultrapure water ($\kappa \leq 0.054\ \mu S\ cm^{-1}$, Millipore®). The suspension was agitating in an ultrasonic bath for 30 min. Then, the ink was sprayed onto the diffusion layer by an air-brush gun fed with pure nitrogen (99.999% purity Praxair), and dried at 70 °C, until a metal amount of 1.0 and 2.0 mg cm^{-2} was loaded at the anode and cathode, respectively. The Nafion® ionomer content in both electrodes was 20 wt.% (dry basis).

Nafion® 115 membranes (DuPont) were pre-treated by boiling first in 3% H_2O_2 for 1 h, then in 0.5 M H_2SO_4 for 2 h, and finally in ultrapure water for 2 h with the water being changed every 30 min. Each MEA was assembled by hot-pressing placing the anode and cathode on either side of the membrane at 50 bar and 130 °C for 180 s.

MEAs were placed into a commercial 5 cm^2 cell hardware (Fuel Cell Technologies, Inc.) which were assembled using a uniform torque of 5 N m. Single cells were operated with a 2.0 M aqueous CH_3OH solution preheated at 60 °C, and pumped through the anode compartment at 1.5 mL min^{-1} and zero back-pressure. Humidified O_2 (99.999% purity, Praxair) at the cell temperature was fed through the cathode compartment at 50 standard $cm^3\ min^{-1}$ (sccm) and zero back-pressure. Polarization curves were registered using a computer controlled home-made DMFC test station, once the MEAs were activated.

Electrochemical impedance spectroscopy measurements were carried out using a Solartron 1287A potentiostat + 1255 FRA. The AC amplitude was 5 mV and the frequency ranged from 100 kHz to 0.01 Hz. From the intercept of the impedance diagrams with the real axis, an apparent electronic resistance of $0.050 \pm 0.05\ \Omega$ was determined for all MEAs used thorough this work.

3. Results and discussion

3.1. Physicochemical characterization of Pd-based catalysts

Table 1 depicts the compositions of catalysts used in the present work, which were determined by energy dispersive X-ray analysis (EDX). Experimental compositions are close to the nominal ones, although lower amount of Ir is perceived. Nominal values of 20 wt.% for metal content on carbon were pretended. However, the introduction of the second and third foreign elements (Fe and Ir) produces a decrease in the metal loading, which may be attributed to a lower anchoring strength on carbon. Structural parameters such as lattice parameter and crystallite size of the catalysts are also included in Table 1. XRD diffractograms of the catalysts show the typical profile of the face centered cubic (fcc) crystalline structure of palladium (Fig. 1) [22,38]. Four diffraction peaks observed at 39.6°, 45.7°, 67.1° and 80.8° are associated with the (1 1 1), (2 0 0), (2 2 0) and (3 1 1) Pd planes, while the diffraction peak at 24.9° is assigned to the graphitic properties of the carbon support [32,23]. The variation of the lattice parameter by the incorporation of a foreign element in the crystalline network of Pd is indicative of alloying formation [39,35]. This effect is more evident for ternary alloy catalysts. Furthermore, the shift of the diffraction peaks toward higher degree values implies a Pd unit cell contraction by alloying it with a foreign element. No other diffraction peaks are visualized. Nonetheless, amorphous metallic oxides cannot be discarded. Fig. 1 and Table 1 also include the XRD patterns and the analysis corresponding to commercial Pd/C and $Pd_{25}Pt_{75}$/C materials. In this context, it is noticeable the strong difference between the nominal and the achieved atomic ratio of the commercial $Pd_{25}Pt_{75}$/C catalyst.

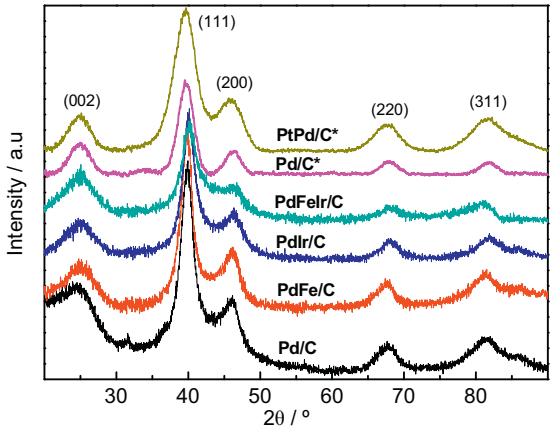

Fig. 1. X-ray diffractograms of commercial* and synthesized materials.

Average crystallite size was calculated employing the Scherrer equation $\left(d = \frac{sk}{b}\cosh\right)$ for the (220) diffraction peak. In this equation d is the average particle size in Å, s is the shape sensitive coefficient (0.9), k is the wavelength of the radiation used (Cu Ka = 1.54056 Å), b is the width at the half of the peak maximum and h is the peak angle [40]. Crystallite size values for all catalysts are similar and vary between 3.4 and 3.9 nm (Table 1). Nevertheless, a close view indicates that the introduction of the second/third element into the Pd/C catalyst slightly decreases the crystallite size and Pd loading, which is in agreement with a previous work [16]. Also, lattice parameter and Pd–$Pd_{(111)}$ interplanar spacing decrease with the alloying degree, and the highest strain effect is achieved by the ternary catalyst.

XPS was used to provide essential information on the oxidation state and the stoichiometry of the elements at the catalyst surface. XPS spectra corresponding to the Pd 3d orbital are reported in Fig. 2a. The Pd 3d signal was deconvoluted into three distin-

Table 1
Composition from EDX and physical parameters from XRD analysis of Pd-based catalysts.

Catalyst	Metal loading (wt.%)	Average particle size (nm)	Lattice parameter (Å)	Atomic ratio (bulk)	Pd–Pd interplanar spacing d (Å)
Pd/C	20	3.9	3.949	100	2.273
PdFe/C	19	3.8	3.922	75:25	2.261
PdIr/C	18	3.7	3.901	82:18	2.247
PdFeIr/C	15	3.4	3.889	49:31:20	2.242
Pd/C[a]	19	3.6	3.904	100	–
$Pd_{25}Pt_{75}$/C[a]	20	2.4	3.918	44:56	–

[a] Commercial catalysts used as anode in DMFC test station.

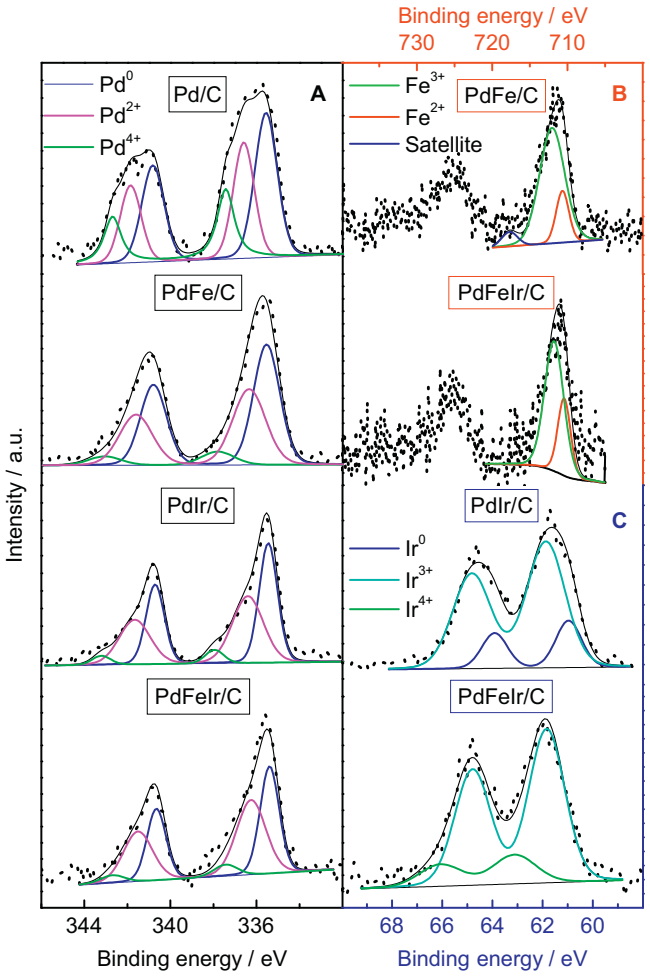

Fig. 2. Pd2d (A), Fe2p (B) and Ir4f (C) core-level spectra of Pd/C, PdFe/C, PdIr/C and PdFeIr/C.

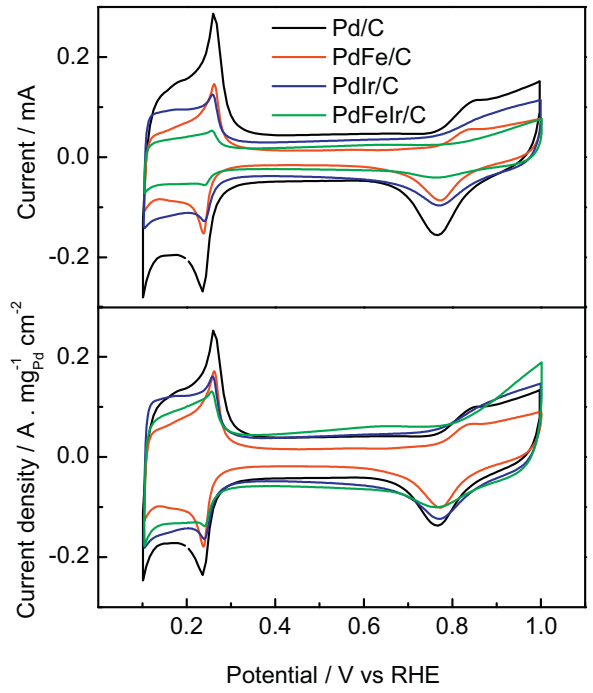

Fig. 3. Blank voltammetry for catalysts in 0.5 M H_2SO_4 at 0.02 V s^{-1}. Current is depicted as measured (top panel) or normalized by the geometric area and mass of Pd (bottom panel).

guishable doublets of different intensity. For the Pd $3d_{5/2}$ transition, the components at 335.3 ± 0.2, 336.3 ± 0.2, 338.1 ± 0.6 eV are attributed to Pd^0, PdO and PdO_2 species, respectively [41]. XPS quantitative analysis for all carbon-supported Pd materials shows an increment and decrement of metallic Pd and PdO_2 species with the metallic alloy formation, which is indicative of charge transfer from the foreign element/s to Pd. The last is supported by the shift toward lower binding energies (BE) of Pd^0 and Pd^{+2} species with the insertion of the foreign element.

The Fe 2p spectrum consists of two signals associated to the $2p_{3/2}$ and $2p_{1/2}$ transitions (Fig. 2b) [42]. The former was deconvoluted in two distinguishable curves of different intensity. Thus, the Fe $2p_{3/2}$ component at 710 ± 0.4 eV is attributed to mixtures of FeO and $Fe(OH)_2$ species (Fe^{2+}), whereas the signal at 711 ± 0.1 is related to Fe^{2+} and Fe^{3+} species richer in the latter, in the form of FeOOH and Fe_3O_4. The shake-up satellites lines at ca. 717.69 eV confirm last species. It is noticeable the rise of Fe^{2+} species at 710 eV and the decrease of the signal at higher energy values (711 eV) at the ternary catalyst. In other words, the introduction of iridium induces a charge transfer to iron and consequently Fe^{2+} species rises. The last is supported by the XPS spectra of Ir 4f orbitals that are depicted in Fig. 2c and their analysis reported in Table 2. Thus, the Ir 4f signal was deconvoluted into three distinguishable doublets of different intensity. The $4f_{7/2}$ peak occurring at B.E. of 60.9, 61.8–61.9 and 63.1 eV were attributed to Ir^0, Ir^{3+} and Ir^{4+} species [43–45]. Noticeable is the absence of metallic iridium in the ternary catalyst surface.

In addition, XPS analysis shows a slight surface increment of iron for the binary and ternary catalysts. The other elements remain similar to those atomic ratios observed for the bulk material by EDX analysis. Thus, carbon supported materials with specific physicochemical properties were obtained and different catalytic activity as well as performance toward the ORR and MOR are expected.

3.2. Electrochemical characterization by cyclic voltammetry

Fig. 3 shows the blank cyclic voltammograms (CVs) for all synthesized catalysts in the supporting electrolyte. Top panel depicts the faradaic currents as they are recorded, whereas the bottom panel illustrates the faradaic current normalized by the mass of Pd into the catalyst. It can be observed that Pd/C reveals the typical profile of Pd polycrystalline, i.e., hydrogen adsorption/desorption and oxide oxidation/reduction regions are clearly observed at $E < 0.4$ V and $E > 0.6$ V, respectively [46]. The voltammetric profile when iron is introduced in the catalyst is similar to that for Pd but lower currents are achieved. It seems that a homogeneous blockage of Pd surface occurs by deposition of other non-active element. On the other hand, an additional effect is observed by Ir introduction in the sample. Firstly, the onset for Pd oxidation is delayed, which is associated to an inhibition of the chemisorption of OH from water dissociation on Pd sites [15,47]. Secondly, the reversible peaks at ca. 0.25 V associated to hydrogen adsorption/desorption on Pd open surface strongly decrease. The last resembles to preferential metal deposition along the Pd open surface sites. However, the effects observed with both foreign materials could be also related to electronic and structural modifications by introduction of other atoms into the crystal structure of Pd. In this sense, an important lattice strain is observed with the insertion of iridium into the metallic alloy. Then, the ternary material develops a voltammetric profile between those observed by PdIr and PdFe catalysts, although the highest inhibition toward the water dissociation (Pd oxide formation) on this material is discerned.

Table 2
Binding energies (e.V.) and relative intensities (%) of the species from XPS.

Element	Palladium			Iron			Iridium			Surface composition
Catalysts	Pd Pd^0	PdO Pd^{2+}	PdO_2 Pd^{4+}	FeO Fe^{2+}	FeO/Fe_2O_3 Fe^{2+}/Fe^{3+}	Satellite Fe^{2+}/Fe^{3+}	Ir^0	Ir_2O_3 Ir^{3+}	Ir_2O_4 Ir^{4+}	
Pd/C	335.5 (43)	336.6 (41)	337.4 (16)	–	–	–	–	–	–	100
PdFe/C	335.5 (52)	336.3 (41)	337.8 (7)	710.7 (18)	712.0 (82)	717.7	–	–	–	54:46
PdIr/C	335.4 (49)	336.4 (46)	337.9 (5)	–	–	–	60.9 (20)	61.9 (80)	–	77:23
PdFeIr/C	335.3 (46)	336.2 (48)	337.4 (6)	710.5 (28)	711.8 (72)	–	–	61.8 (82)	63.1 (18)	47:35:18

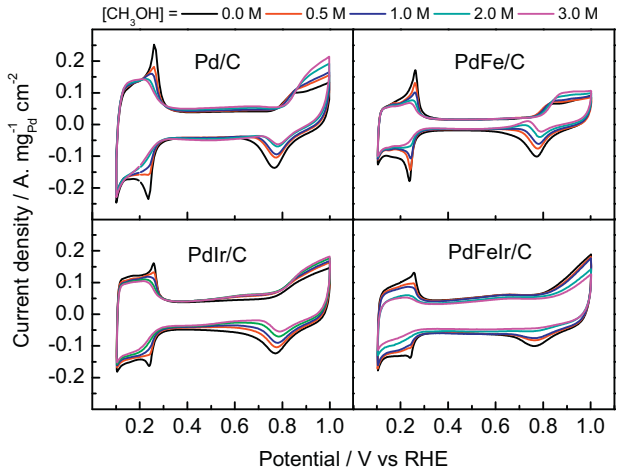

Fig. 4. Cyclic voltammograms for catalysts in 0, 0.5, 1, 2 and 3 M CH_3OH + 0.5 M H_2SO_4 solution at 0.02 V s^{-1}.

Also a reduction of the double layer charge (capacitive currents) with the introduction of iron in the sample is evidenced. The last can be related to faster kinetic of electron transfer or to a reduction of the porosity of the material. It is reasonable to attribute this effect to a lower resistance of the electronic transfer by Fe species on the surface due to the main porosity of the sample is delivered by the catalyst support, which is the same for all catalysts.

In this context, in reference [16] Pd/C, Pd_3Fe/C and Pd_2FeIr/C catalysts were prepared via an organic colloid method in an ethylene glycol (EG) solution, and the electrochemical profiles of the catalysts in perchloric acid for those materials are somehow different to the achieved in the current work. Main differences may reside in the counter anion (perchlorate instead of sulphate) and the different synthetic routes to prepare the catalysts.

Fig. 4 shows the catalytic activity toward methanol oxidation for all catalysts in absence of oxygen. First of all, a poor catalytic activity toward alcohol oxidation for all Pd-based catalysts can be established. Nonetheless, the rise in alcohol concentration inhibits the hydrogen adsorption/desorption at ca. 0.25 V and Pd oxide formation on the materials. The last can be discerned from the lower charge of the cathodic peak at ca. 0.8 V associated to the reduction of Pd oxide with the rise of alcohol concentration. In addition, methanol oxidation can be distinguished as an anodic contribution at $E > 0.5$ V for PdIr/C and at $E > 0.8$ V for Pd/C and PdFe/C electrodes during the positive scan and as a mix current (methanol oxidation + Pd oxide reduction) during the cathodic scan at potential lower than 0.8 V. The last is clear for PdFe/C materials, although a small but visible anodic features can be discerned at Pd/C and PdIr/C electrodes during the cathodic sweep. Remarkably, the three-metallic catalyst does not oxidize methanol, but it adsorbs on the catalyst surface inhibiting the hydrogen adsorption and water dissociation reactions. These effects can be established from the decrease in the currents associated to the hydrogen adsorption/desorption at $E < 0.4$ V and Pd oxide formation/reduction reactions at $E > 0.6$ V with the rise of the methanol concentration.

These results are of paramount importance due to physicochemical parameters control the mechanism and rate of water dissociation and methanol oxidation reactions. Dilution of the active site could be invoked to understand the activity toward the methanol oxidation reaction, since Pd loading decreases in the following way: 225 μg cm^{-2} (Pd/C) > 165 μg cm^{-2} (PdFe/C) > 156 μg cm^{-2} (PdIr/C) > 80 μg cm^{-2} (PdFeIr/C). Nevertheless, it cannot be the main responsible for the observed due to iron segregates to the catalyst surface and therefore PdFe/C materials may present the highest Pd dilution effect. Contrary to expectations, PdFe/C is one of the most active materials for the alcohol oxidation reaction. Surface structure and electronic considerations may explain the experimental results. In this sense, metallic Pd atoms forming an open surface structure strongly decrease with Ir insertion and thus the activity toward the methanol oxidation reaction. The last is supported by the XRD analysis in which the lattice parameter and therefore lattice strain increase with Fe and specially with Ir introduction into the catalytic material. It is noticeable that methanol essentially adsorbs on Pd open surface sites for Pd/C, PdFe/C and PdIr/C materials. A complete different behavior is observed for the ternary catalyst in which a preferential methanol adsorption site is not perceived and that the hydrogen adsorption state is almost inhibited with the highest methanol concentration used. Moreover, methanol does not oxidize on the ternary catalyst in the working potential range, and Pd oxides formation is inhibited by methanol adsorption. Therefore, surface structure parameters such as the most packed surface and the lowest particle size in conjunction with electronic considerations like the absence of metallic iridium make the ternary catalyst unique.

3.3. *Electrochemical characterization by rotating disk electrode (RDE)*

In order to evaluate the catalytic activity toward the ORR on the synthesized materials in absence and presence of methanol, RDE experiments were carried out. Fig. 5 shows polarization curves recorded at 1600 rpm in absence (a) and presence of alcohol (b and c) for all carbon supported catalysts. In order to clarify and stress the alcohol effect, only the lowest (0.5 M) and the highest (3 M) alcohol concentrations are depicted in Fig. 5. Two typical potential regions can be discerned; (i) at high overpotentials ($E < 0.5$ V), in which the reaction is controlled by diffusion of O_2 toward the catalytic surface, and (ii) at low overpotentials ($E > 0.5$ V), in which the reaction is governed by kinetic and diffusion processes [48]. The left panels of Fig. 5 assume that all catalysts have the same amount of active sites with same behavior toward alcohol tolerance (surface blockage) at low potentials (0.2 V), and therefore their current intensities were matched at this potential. In this way, it is easy to analyze the ORR activity and the alcohol tolerance for each catalyst in the low overpotential region (1.0–0.5 V). First of all, it is observed that all Pd-based catalysts develop higher alcohol tolerance than Pt-based materials [15,16]. Secondly, bi- and tri-metallic catalysts improve the ORR in absence and presence of methanol respect to Pd/C material, but some differences can be established between

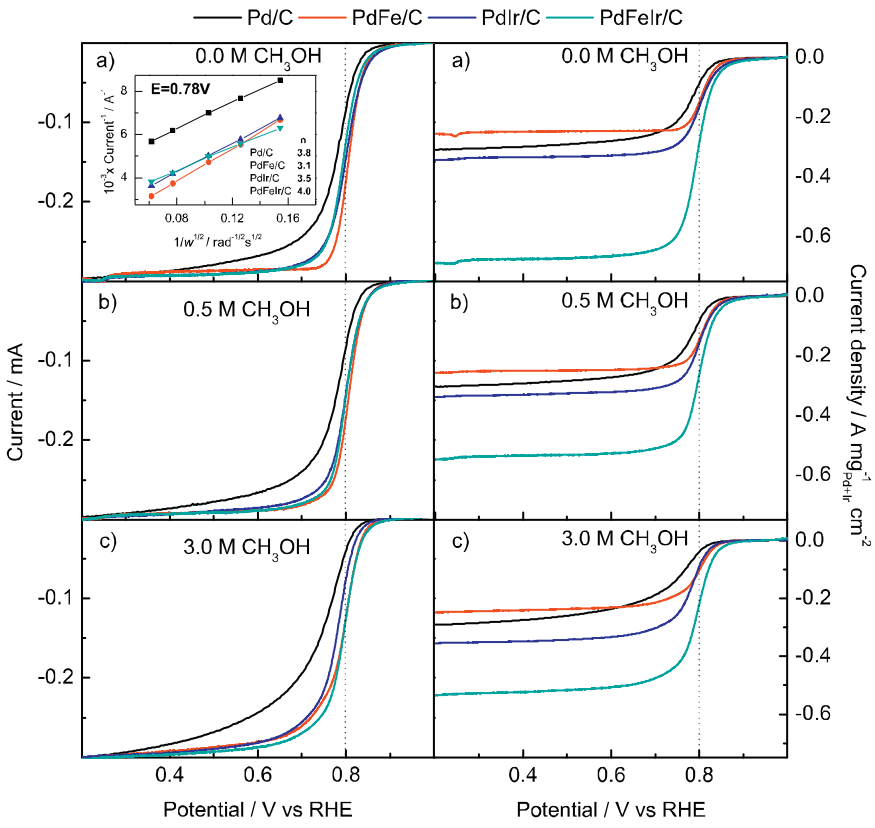

Fig. 5. Linear sweep voltammetry curves for catalysts recorded in 0, 0.5, 1, 2 and 3 M CH_3OH + 0.5 M H_2SO_4 solution at 1600 rpm and 2 mV s^{-1}. Current is depicted as measured (left panels) or normalized by the geometric area and the mass of noble metals (right panels).

Table 3
Efficiencies of the DMFCs from the top panel of Fig. 6 at 0.1 A cm^{-2}.

MEA	Cell voltage @ 0.1 A cm^{-2} (V)	η_V (%)	η (%)
PdFeIr	0.40	34	32
$Pd_{25}Pt_{75}$[a]	0.34	29	28
Pd[a]	0.29	25	24

[a] Commercial catalysts.

them. Thus, PdFe/C develops the highest activity toward the ORR in absence of alcohol, but its performance decreases with the alcohol concentration. On the other hand, the current profile delivered by the PdIr/C material remains similar in the presence of alcohol, but the intensity decreases with the alcohol concentration. Finally, the ternary catalyst is the material with the major methanol tolerance and therefore it develops the highest performance toward the ORR at the highest alcohol concentration (left panel of Fig. 5c), in accord with a previous work [16]. Remarkably is the agreement with the previous voltammetric experiments, in which the highest tolerance to methanol was achieved with the tri-metallic catalyst (Fig. 4). Therefore, the catalytic activity toward the ORR in presence of high alcohol concentration (3 M) follows the subsequent order: PdFeIr/C > PdFe/C > PdIr/C > Pd/C.

The right panels of Fig. 5 shows the same experiments than those depicted in the left panels, but the currents are normalized with respect to the amount of mass of both noble metals (Pd + Ir) and the geometric area, and therefore the mass activity of the precious metals can be discerned. The highest mass activity of the tri-metallic catalysts toward the ORR in absence and presence of alcohol in the solution is clearly observed. Independently of the alcohol concentration, the mass activity toward the ORR follows the subsequent trend: PdFeIr/C > PdFe/C > PdIr/C > Pd/C.

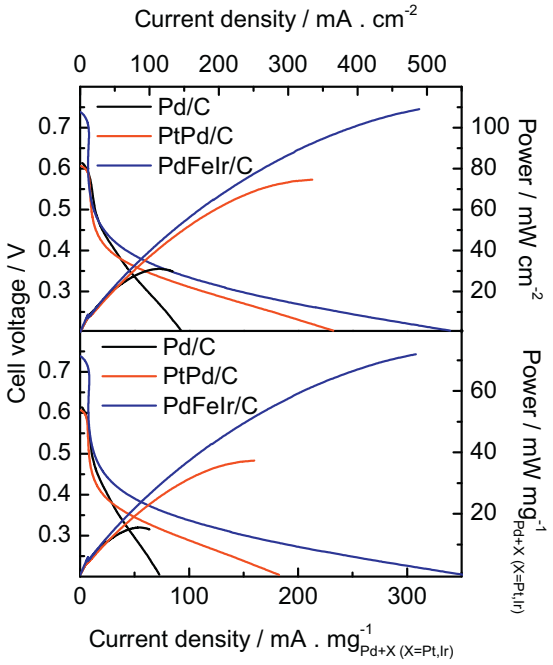

Fig. 6. Voltage vs Current and Power vs Current curves for single DMFC. Current and Power are depicted as measured (top panel) and normalized by the mass of noble metals (bottom panel). Cathode catalyst: Pd, PdPt and PdFeIr at loading of 2.0 mg_{metal} cm^{-2}. Anode: PtRu/C at loading 1.0 mg_{metal} cm^{-2}. T_{cell} = 60 °C. Anode fed with 2.0 M CH_3OH and 1.5 mL min^{-1}. Cathode fed with humidified O_2 at 50 mL min^{-1}.

Another important issue is the mechanism and the kinetic of the ORR occurring at the catalysts. However, this subject is out of the current work and only main results are indicated. Thus, according to the Koutecky–Levich theory the electron transfer number during the ORR process is close to four for all catalysts, which indicates that oxygen is fully reduced at the electrode surfaces (inset of Fig. 5a).

Therefore, results depicted at Figs. 4 and 5 indicate an elevated activity toward the ORR and high methanol tolerance of the ternary catalyst, which may produce a high reduction cost of the catalytic material. In this context, it is important to note that methanol acts as simple "third body effect" at this material, in which the adsorbed molecules block the surface sites but does not oxidize, and consequently a better performance as cathode in a DMFC is expected, i.e., the mixed potential at the cathode should be avoided.

3.4. Test in single direct methanol fuel cell (DMFC)

The top panel of Fig. 6 shows the voltage–current density and power–current density curves registered in the single DMFC operating with a 2 M aqueous methanol at 60 °C and atmospheric pressure for the MEA with a composition PtRu/C|N115|PdFeIr/C. The cathode was fed with pure O_2 to maximize its activity. In addition, polarization curves corresponding to commercial Pd/C as reference and commercial $Pd_{25}Pt_{75}$/C that develops the highest catalytic activity toward ORR in presence of methanol [49–51] were included as comparison.

It is apparent that the open circuit voltage (OCV) given by the MEA with PdFeIr/C catalyst is around 0.125 V higher than those given by the MEAs with Pd/C and $Pd_{25}Pt_{75}$/C catalysts. This indicates that the trimetallic catalyst has improved tolerance toward methanol oxidation, because the methanol crossover is highest at the OCV [52]. This result is in agreement with those observed in half-cell configuration in which methanol adsorbs but it does not oxidize on the ternary catalyst. Indeed, the improved methanol tolerance directly affects the OCV in which the voltage loss by the "mixed potential" effect decreases at the ternary catalysts.

The best performance was obtained from the MEA that incorporated the PdFeIr/C catalyst. Thus, at a practical voltage of 0.350 V the current density delivered by this MEA was 0.130 A cm^{-2} (45.5 mW cm^{-2}), while the MEAs with $Pd_{25}Pt_{75}$/C and Pd/C delivered 0.094 (32.9 mW cm^{-2}) and 0.071 (24.8 mW cm^{-2}) A cm^{-2}, respectively. Furthermore, the behavior of the catalysts in the single DMFC reflects the results of anode polarization experiments found in MEAs. This could be tentatively extended to previous results in the literature obtained in three-electrode cells to predict a good approach when applied to real fuel cells.

To gain more insight about the fuel cell properties in the operating region of the polarization curve, it is possible to estimate the overall efficiency of the DMFCs, under the conditions that the methanol oxidation gives 6 mol e^-/mol CH_3OH [53,54], which is equal to:

$$\eta = \eta_{\text{rev.}} \times \eta_V$$

where $\eta_{\text{rev.}}$ is the thermodynamic efficiency of the reaction taking place in the DMFC (0.967) under standard conditions [53,54], and η_V is the voltage efficiency. The latter is defined as:

$$\eta_V = \frac{\Delta V}{\Delta E_{\text{rev.}}}$$

where ΔV is the actual fuel cell voltage at given current density and $\Delta E_{\text{rev.}}$ is the electromotive force at the same temperature and pressure (approximately 1.18 V) [53,54]. According to the data reported in Table 3, the use of a cathode with enhanced activity and specificity toward the ORR, like PdFeIr/C, positively influence the DMFC efficiency.

Furthermore, the bottom panel of Fig. 6 shows the voltage and power vs current curves but normalized by the total noble-metal mass activity, which is of paramount importance in a practical and economical point of view. Accordingly, the ternary catalyst in comparison to Pd/C and $Pd_{25}Pt_{75}$/C developed a rise of 146% and 87% in terms of current and power density at 0.35 V.

Consequently, a low-cost material with enhanced activity and specificity toward the ORR was developed. Since PdFeIr/C carries higher catalytic activity and specificity comparing with commercial Pd/C and $Pd_{25}Pt_{75}$/C, less precious metal will be required for higher performance and it will in turn reduce the cost of fuel cell materials, e.g., in the current conditions the cathodic material cost is reduced until a 79% respect with PdPt/C and a 46% to Pd/C catalyst. The improvement in both power output and OCV is related to the third-body effect of methanol on the ternary catalyst that is produced by electronic and geometric factors, which is for our knowledge the first time acquired in DMFC.

4. Conclusions

In the present work, low-cost carbon-supported Pd and Pd-based alloys (PdFe/C, PdIr/C, PdFeIr/C) with elevated catalytic activity and high specificity toward the ORR were successfully synthesized by the borohydride method to be used as cathodic material in a DMFC.

Physicochemical characterization indicated similar crystallite size of ca. 4 nm for all catalysts. In addition, XRD and XPS analysis showed the importance of the alloy formation and the electronic charge transfer from Fe and/or Ir to Pd. Thus, voltammetric analysis revealed the high impact of the material surface structure for the catalysis, in which methanol adsorbs but not oxidize on the PdFeIr/C catalyst. Furthermore, it was observed that iridium introduction into the Pd-based catalyst enhance the methanol tolerance and inhibits the water dissociation reaction and hence the oxidation of the catalyst surface. Indeed, absence of metallic iridium (Ir^0) and presence of iron (Fe^{2+} and Fe^{3+}) and iridium (Ir^{+3} + Ir^{+4}) oxides into specific surface sites are the key species for the enhanced activity toward the ORR in presence of dissolved methanol. Consequently, the best performance in DMFC was achieved with a cathode containing PdFeIr/C catalyst.

These results are of paramount importance since the development of good and low-cost catalysts for ORR in the presence of alcohol is crucial for the introduction of direct methanol fuel cells in the energy market.

Acknowledgments

The authors gratefully acknowledge financial support given by the Spanish MINECO under projects CTQ2011-28913-C02-02 and ENE2014-52158-C2-2-R (co-funded by FEDER).

References

[1] L. Carrette, K.A. Friedrich, U. Stimming, ChemPhysChem 128 (2000) 162–193.
[2] F. Segura, J.M. Andu, Renew. Sustain. Energy Rev. 13 (2009) 2309–2322.
[3] B.L. Carrette, K.A. Friedrich, U. Stimming, Fuel Cells 1 (2001) 5–39.
[4] S.K. Kamarudin, W.R.W. Daud, S.L. Ho, U.A. Hasran, J. Power Source 163 (2007) 743–754.
[5] S.K. Kamarudin, F. Achmad, W.R.W. Daud, Int. J. Hydrog. Energy 34 (2009) 6902–6916.
[6] E. Antolini, J. Power Sources 170 (2007) 1–12.
[7] F.A. De Bruijn, V.A.T. Dam, G.J.M. Janssen, Fuel cells 1 (2008) 3–22.
[8] X. Li, A. Faghri, J. Power Sources 226 (2013) 223–240.
[9] E. Antolini, J.R.C. Salgado, L.G.R.A. Santos, G. García, E.A. Ticianelli, E. Pastor, E.R. Gonzalez, J. Appl. Electrochem. 36 (2006) 355–362.
[10] M.Z.F. Kamarudin, S.K. Kamarudin, M.S. Masdar, W.R.W. Daud, Int. J. Hydrog. Energy 38 (2013) 9438–9453.
[11] S. Koh, P. Strasser, J. Am. Chem. Soc. 129 (2007) 12624–12625.

[12] S. Kondo, M. Nakamura, N. Maki, N. Hoshi, J. Phys. Chem. C 113 (2009) 12625–12628.
[13] H. Liu, A. Manthiram, Energy Environ. Sci. 2 (2009) 124–132.
[14] A.V. Martínez, M.T. Rodríguez, M.G. Arzaluz, Int. J. Electrochem. Sci. 7 (2012) 7140–7151.
[15] M. Neergat, V. Gunasekar, R. Rahul, J. Electroanal. Chem. 658 (2011) 25–32.
[16] R. Wang, S. Liao, Z. Fu, S. Ji, Electrochem. Commun. 10 (2008) 523–526.
[17] S. Bah, O. Savadogo, J. Electroanal. Chem. 636 (2009) 1–9.
[18] C. Bianchini, P.K. Shen, Chem. Rev. 109 (2009) 4183–4206.
[19] M. Shao, K. Sasaki, R.R. Adzic, J. Am. Chem. Soc. 128 (2006) 3526–3527.
[20] M.H. Shao, T. Huang, P. Liu, J. Zhang, K. Sasaki, M.B. Vukmirovic, R.R. Adzic, Langmuir 22 (2006) 10409–10415.
[21] X. Wang, Y. Tang, Y. Gao, T. Lu, J. Power Source 175 (2008) 784–788.
[22] W. Wang, D. Zheng, C. Du, Z. Zou, X. Zhang, B. Xia, H. Yang, D.L. Akins, J. Power Source 167 (2007) 243–249.
[23] E. Antolini, Energy Environ. Sci. 2 (2009) 915–931.
[24] W. Pan, X. Zhang, H. Ma, J. Zhang, J. Phys. Chem. C 112 (2008) 2456–2461.
[25] V. Raghuveer, P.J. Ferreira, A. Manthiram, Electrochem. Commun. 8 (2006) 807–814.
[26] Z. Peng, H. Yang, J. Am. Chem. Soc. 131 (2009) 7542–7543.
[27] V. Raghuveer, A. Manthiram, A.J. Bard, J. Phys. Chem. B 109 (2005) 22909–22912.
[28] C.V. Rao, B. Viswanathan, Electrochim. Acta 55 (2010) 3002–3007.
[29] R.G. Raptis, C.R. Cabrera, ACS Appl. Mater. Interfaces 5 (2013) 11603–11612.
[30] L. Shen, H. Li, L. Lu, Y. Luo, Y. Tang, Y. Chen, T. Lu, Electrochim. Acta 89 (2013) 497–502.
[31] D.N. Son, K. Takahashi, J. Phys. Chem. C 116 (2012) 6200–6207.
[32] Y. Tang, S. Cao, Y. Chen, T. Lu, Y. Zhou, L. Lu, J. Bao, Appl. Surf. Sci. 256 (2010) 4196–4200.
[33] L. Zhang, K. Lee, J. Zhang, Electrochim. Acta 52 (2007) 7964–7971.
[34] M. Ramanathan, V. Ramani, J. Prakash, Electrochim. Acta 75 (2012) 254–261.
[35] J. Zhang, Y. Mo, M.B. Vukmirovic, R. Klie, K. Sasaki, R.R. Adzic, J. Phys. Chem. C 108 (2004) 10955–10964.
[36] H. Ma, X. Xue, J. Liao, C. Liu, W. Xing, Appl. Surf. Sci. 252 (2006) 8593–8597.
[37] F.I. Pires, H.M. Villullas, Int. J. Hydrog. Energy 37 (2012) 17052–17059.
[38] W. Vogel, J. Phys. Chem. C 115 (2011) 1506–1512.
[39] E. Antolini, S.C. Zignani, S.F. Santos, E.R. Gonzalez, Electrochim. Acta 56 (2011) 2299–2305.
[40] E.F.A. Zeid, D.K. Hee, S. Lee, Y. Kim, J. Appl. Electrochem. 40 (2010) 1917–1923.
[41] W. Zhou, M. Li, O.L. Ding, S.H. Chan, L. Zhang, Y. Xue, Int. J. Hydrog. Energy 39 (2014) 6433–6442.
[42] A.P. Grosvenor, B.A. Kobe, M.C. Biesinger, N.S. Mcintyre, Surf. Interface Anal. 36 (2004) 1564–1574.
[43] S.Y. Shen, T.S. Zhao, J.B. Xu, Electrochim. Acta 55 (2010) 9179–9184.
[44] D. Labou, E. Slavcheva, U. Schnakenberg, S. Neophytides, J. Power Source 185 (2008) 1073–1078.
[45] P. van der Heide, X-Ray Photoelectron Spectroscopy. An Introduction to Principles and Practice, John Wiley & Sons, Inc., New Jersey, United States of America, 2012.
[46] C.A. Grde Michal, L. Mariusz, J. Gregory, Electrochim. Acta 53 (2008) 7583–7598.
[47] K. Lee, O. Savadogo, A. Ishihara, S. Mitsushima, N. Kamiya, K. Ota, J. Electrochem. Soc. 153 (2006) A20–A24.
[48] M.H. Shao, T. Huang, P. Liu, J. Zhang, K. Sasaki, M.B. Vukmirovic, R.R. Adzic, Langmuir 22 (2006) 10409–10415.
[49] Q.X.H. Li, G. Sun, N. Li, S. Sun, D. Su, J. Phys. Chem. 111 (2008) 5605–5617.
[50] X.L.Y. Xu, J. Power Sources 170 (2007) 3627–3633.
[51] H. Ye, R.M. Crooks, J. Am. Chem. Soc. 129 (2007) 3627–3633.
[52] R. Marchesi, P. Grassini, A. Casalegno, Appl. Therm. Eng. 27 (2007) 748–754.
[53] C. Lamy, J.-M. Léger, Advanced electrode materials for the direct methanol fuel cell, in: A. Wieckowski (Ed.), Interfacial Electrochemistry. Theory, Experiment, and Applications, Marcel Dekker, Inc., New York, 1999, p. 885, Ch. 48.
[54] A.S. Arico, V. Baglio, V. Antonucci, Direct methanol fuel cells: history, status and perspectives, in: H. Liu, J. Zhang (Eds.), Electrocatalysis of Direct Methanol Fuel Cells: from Fundamentals to Applications, Wiley-VCH Verlag GmbH & Co. KGaA, Weinheim, 2009, pp. 3–9, Ch. 1.